Treatment Potential for *LCA5*-Associated Leber Congenital Amaurosis

Katherine E. Uyhazi,[1,2] Puya Aravand,[1] Brent A. Bell,[1] Zhangyong Wei,[1] Lanfranco Leo,[1] Leona W. Serrano,[2] Denise J. Pearson,[1,2] Ivan Shpylchak,[1] Jennifer Pham,[1] Vidyullatha Vasireddy,[1] Jean Bennett,[1] and Tomas S. Aleman[1,2]

[1]Center for Advanced Retinal and Ocular Therapeutics (CAROT) and F.M. Kirby Center for Molecular Ophthalmology, University of Pennsylvania, Philadelphia, PA, USA
[2]Scheie Eye Institute at The Perelman Center for Advanced Medicine, University of Pennsylvania, Philadelphia, PA, USA

Correspondence: Tomas S. Aleman, Perelman Center for Advanced Medicine, University of Pennsylvania, 3400 Civic Center Blvd, Philadelphia, PA 19104, USA; aleman@pennmedicine.upenn.edu.

Received: November 19, 2019
Accepted: March 16, 2020
Published: May 19, 2020

Citation: Uyhazi KE, Aravand P, Bell BA, et al. Treatment potential for *LCA5*-associated Leber congenital amaurosis. *Invest Ophthalmol Vis Sci.* 2020;61(5):30. https://doi.org/10.1167/iovs.61.5.30

Purpose. To determine the therapeutic window for gene augmentation for Leber congenital amaurosis (LCA) associated with mutations in *LCA5*.

Methods. Five patients (ages 6–31) with LCA and biallelic *LCA5* mutations underwent an ophthalmic examination including optical coherence tomography (SD-OCT), full-field stimulus testing (FST), and pupillometry. The time course of photoreceptor degeneration in the *Lca5*$^{gt/gt}$ mouse model and the efficacy of subretinal gene augmentation therapy with AAV8-*hLCA5* delivered at postnatal day 5 (P5) (early, n = 11 eyes), P15 (mid, n = 14), and P30 (late, n = 13) were assessed using SD-OCT, histologic study, electroretinography (ERG), and pupillometry. Comparisons were made with the human disease.

Results. Patients with *LCA5*-LCA showed a maculopathy with detectable outer nuclear layer (ONL) in the pericentral retina and at least 4 log units of dark-adapted sensitivity loss. The *Lca5*$^{gt/gt}$ mouse has a similarly severe and rapid photoreceptor degeneration. The ONL became progressively thinner and was undetectable by P60. Rod- and cone-mediated ERGs were severely reduced in amplitudes at P30 and became nondetectable by P60. Subretinal AAV8-*hLCA5* administered to *Lca5*$^{gt/gt}$ mice at P5 and P15, but not at P30, resulted in structural and functional rescue.

Conclusions. *LCA5*-LCA is a particularly severe form of LCA that was recapitulated in the *Lca5*$^{gt/gt}$ mouse. Gene augmentation resulted in structural and functional rescue in the *Lca5*$^{gt/gt}$ mouse if delivered before P30. Retained photoreceptors were visible within the central retina in all patients with *LCA5*-LCA, at a level equivalent to that observed in rescued *Lca5*$^{gt/gt}$ mice, suggesting a window of opportunity for the treatment of patients with *LCA5*-LCA.

Keywords: LCA5, lebercilin, leber congenital amaurosis, gene therapy, AAV8

Leber congenital amaurosis (LCA) is a molecularly heterogeneous, early-onset, severe inherited retinal degeneration that typically presents within the first year of life with nystagmus and profound vision loss. LCA has been associated with mutations in more than 25 genes [Retnet: https://sph.uth.edu/retnet/] that are essential for photoreceptor and retinal pigment epithelium (RPE) function. One such gene, *Lebercilin (LCA5),* accounts for approximately 2% of LCA cases and results in a particularly severe form of the disease.[1–15] The *LCA5* gene (also known as *C6ORF152)* located in chromosome 6q14.1 encodes an 80 kDa protein expressed in the connecting cilium of photoreceptors.[3] Lebercilin interacts with other intraflagellar transport proteins required for the bidirectional movement of proteins from the inner to outer segments of photoreceptors and is necessary for photoreceptor outer segment formation.[7,16,17] In the *Lca5*$^{gt/gt}$ mouse model of the disease, homozygous null *Lca5* gene trap (gt) insertions cause a severe retinal degeneration within a few weeks of birth.[16,18] At postnatal day (P) 12, the outer nuclear layer (ONL) is normal in thickness, but the photoreceptor inner and outer segments (POS) are already shorter than normal.[16] By P28 the ONL thins to about one third of normal with only 3 or 4 rows of nuclei. At P60 only a single row of ONL remains, which is no longer observable by 4 months.[16] Both scotopic and photopic electroretinogram (ERG) responses have been reported as undetectable by P25.[16]

The remarkable success of Luxturna (voretigene neparvovec-rzyl; Spark Therapeutics, Philadelphia, PA, USA), the first gene therapy product approved by the Food and Drug Administration for an inherited retinal degeneration (IRD) (*RPE65-LCA*), has energized the search for treatments for other molecular forms of IRDs.[19,20] We have previously shown that a recombinant adeno-associated viral vector (AAV7m8) containing human *LCA5* cDNA can rescued ONL thickness, pupillary responses, and water maze performance when delivered to the subretinal space of neonatal *Lca5*$^{gt/gt}$ mice.[16,18] Of note, these injections

were performed in P4–P6 mice before retinal degeneration had started and thus is not translatable to the early phases of eventual human clinical trials. Patients with *LCA5*-LCA typically show a moderate to severe retinal degeneration by the time they are diagnosed early in life. In this work we performed AAV-mediated rescue experiments in $Lca5^{gt/gt}$ mice at time points when photoreceptor degeneration is well under way, better modeling the structural and functional phenotype of patients who may be considered for enrollment in the early phases of future human clinical trials.

Methods

Human Studies

Five patients ages 6 to 31 years (hereafter referred to as Patients 1–5, P1–P5*)*, diagnosed with LCA caused by biallelic null mutations in *LCA5* underwent a comprehensive eye examination. The data were obtained from the patients' clinical records. Retinal imaging was performed with spectral domain optical coherence tomography (SD-OCT) and when possible with near-infrared reflectance (NIR-REF) and fundus autofluorescence (FAF) with NIR and short-wavelength (SW) excitation lights (Spectralis, Heidelberg Engineering, Carlsbad, CA). Wide-field retinal imaging was performed (Optos, Inc., Marlborough, MA) in one patient. SD-OCT imaging was performed with 9 mm-long horizontal sections crossing the anatomic fovea; our scanning protocol, analyses, and normative data have been published.[21–23] In brief, segmentation of SD-OCT images was done both with the built-in segmentation software of the Spectralis OCT system and with ImageJ analysis software (http://imagej.nih.gov/ij/links.html) using longitudinal reflectivity profile (LRP) analyses. Retinal thickness was defined as the distance between the signal peak at the vitreoretinal interface (the internal limiting membrane, ILM) and the posterior boundary of the major signal peak that corresponds to the basal retinal pigment epithelium/Bruch's membrane (RPE/BrM). In normal subjects, the RPE/BrM is the last reflectivity within the four to six signals that are identifiable in the outer retina. In patients, the presumed RPE signal was often the only signal in the outer retina merging with signals from the anterior choroid. To avoid ambiguities in the determination of the external limiting membrane in severely degenerated regions, the term "outer retinal thickness" was adopted to define the thickness between the outer plexiform layer (OPL) and RPE/BrM. Inner retinal thickness was defined as the distance between the ILM and the OPL. Visual sensitivity was measured in dilated, dark-adapted patients using full-field stimulus testing (FST).[24,25] All patients were able to complete FST testing except patient 1 (P1, 6 years old). Results in P3 were highly variable and considered unreliable and thus were excluded from analysis. The direct transient pupillary light reflex (TPLR) was elicited by full-field, 100 ms chromatic stimuli delivered by a Ganzfeld simulator of a full-field electroretinography system (ColorDome, Espion E^3; Diagnosys, Lowell, MA, USA) connected to an eye-tracker (EyeFrame; Arrington Research, Scottsdale, AZ, USA) and software (VoltagePoint; Arrington Research) as previously described.[21] TPLR luminance response functions were recorded with increasing intensities of scotopically matched blue (467 nm) and red (637 nm) lights presented at 0.5 log unit increments in the dark-adapted state. Four-second video clips were recorded after each stimulus, which were used to manually measure pupil diameter in these patients with large-amplitude nystagmus that interfered with automated tracking. Informed consent was obtained; all procedures followed institutional guidelines protocol numbers 815348 and 832468) and complied with the Declaration of Helsinki.

Murine Studies

Husbandry and Study Design. All animals were bred and maintained in the animal facilities of The University of Pennsylvania under a 12-hour light (993 lux)/12-hour dark cycle with free access to food and water. Experiments were conducted in accordance with federal and institutional regulations on IACUC protocol no. 805890 and with the ARVO Statement for the Use of Animals in Ophthalmic and Vision Research. Animals were anesthetized with intraperitoneal ketamine (87.5 mg/kg) and xylazine (10 mg/kg). Corneas were anesthetized with topical 0.5% proparacaine hydrochloride (Akron, Lake Forest, IL, USA), and pupils were dilated with topical 0.5% tropicamide/phenylephrine hydrochloride combination drops (Mydrephrine P; Nitto Medic Co., Ltd., Japan). Media opacities were minimized by ocular eye shields[26] in conjunction with artificial tears (Refresh; Allergan, Irvine, CA, USA). Mice were recovered on a heated pad (Homeothermic Monitor/Blanket Product No. 507220F; Harvard Apparatus, Holliston, MA, USA) with the eyes coated with Puralube Vet ophthalmic ointment (Dechra Veterinary Products, Overland Park, KS, USA).[27]

Subretinal Injections. AAV vectors were generated and purified in the research vector core of the Center for Advanced Retinal and Ocular Therapeutics (CAROT) at the University of Pennsylvania. Because of decreased expression and increased toxicity of the AAV7m8 vector in the nonhuman primate retina, wild-type *LCA5* was delivered using a well-characterized AAV8 serotype that has a more favorable safety and expression profile in both mouse and primate retina.[28–30] The AAV8-h*LCA5* vector contains a full-length human native *LCA5* cDNA under the control of the hybrid CMV-chicken β-actin promoter to drive ubiquitous expression in transduced retinal cells.[3,18] Vectors were generated by triple transfection and delivered in excipient containing phosphate-buffered saline solution (PBS) with 0.001% Pluronic F68 (PF68).[31] Bilateral subretinal injections were performed in P5, P15, and P30 $Lca5^{gt/gt}$ mice using previously described methods with modification.[32] Briefly, an incision was created just posterior to the temporal limbus with a 30 -gauge disposable needle. A 33-gauge, blunt, unbeveled needle on a 5-µL Hamilton syringe (Hamilton Co, Reno, NV, USA) was introduced through the incision and advanced posterior to the lens into the subretinal space. One microliter of a solution containing AAV8-hLCA5 was injected into the subretinal space, delivering 1.0E+09 viral genomes (vg) per eye, an optimal dose based on previous expression and toxicity profiling studies.[18] Control injections were performed with excipient only. Pred-G ophthalmic ointment (Allergan) was applied to the eyes immediately after the procedure. Surgical complications included retinal hemorrhage, retinal detachment, and cataract, as identified by indirect ophthalmoscopy and optical coherence tomography (OCT). Retinal hemorrhages were small and resolved spontaneously. Retinal detachments persisted throughout the study (to P60) but did not interfere with testing. Eyes with dense cataracts that interfered with imaging and functional studies (one eye in

Investigative Ophthalmology & Visual Science

the P5-treated cohort and two eyes from the P30-treated cohort) were excluded from further analysis.

Retinal Imaging. An SD-OCT system (Bioptigen Model R2200 Envisu; Leica Microsystems, Buffalo Grove, IL, USA) was used to obtain orthogonal radial volume scans (1.4-mm; 1000 A/scans × 2 B-scans × 15 frames @ 0° and 90° orientation) and averaged B-scans (15 frames) of the retina from the central (optic nerve centrally positioned within the en-face image), temporal, nasal, superior, and inferior quadrants. After acquisition, images underwent coregistration and averaging using Bioptigen Envisu Software v2.1. Images were exported as bitmaps to imaging analysis software (ImageJ). The ONL was defined as the hyporeflective band between the OPL and the external limiting membrane. ONL thickness was measured at two locations per eye in uninjected *Lca5*$^{gt/gt}$ and wild-type mice (200 µm nasal and temporal to the optic nerve) and at two locations within regions with detectable ONL in the nasal retina of treated animals (at the site of the subretinal injection), at a location that corresponded to the nasal measurements of uninjected *Lca5*$^{gt/gt}$ and wild-type animals.

Electroretinography and Pupillometry. Animals were dark-adapted overnight before testing. At 30 or 60 days after treatment, animals were anesthetized and dilated as above and placed on a 37-degree stage. Custom-made clear plastic contact lens electrodes were placed over each eye, and a platinum wire loop reference electrode was placed in the animal's mouth. Full-field ERGs were recorded using a custom-built Ganzfeld dome and a computer-based system (Espion E2; Diagnosys) in a climate-controlled, electrically isolated dark room under dim red illumination. Band-pass filter cutoff frequencies were 0.3 Hz and 300 Hz. Experiments were started with dark-adapted ERGs elicited with increasing intensities of blue (467 nm; −4.5 log scot-cd.s.m^{-2} to +1.9 log scot-cd.s.m^{-2} in 0.5 log unit steps) to single flash stimuli averaged at 0.5 Hz, as well as with 4-Hz and 10-Hz flicker stimuli.[33] Separate intensity series were recorded, starting with the single flash (0.5 Hz) series, followed by the 4-Hz and then the 10-Hz series; 10 to 20 responses were averaged for each of the intensity steps. Amplitudes and timings of the a- and b-wave amplitudes, as well as of the peak amplitude of the flicker ERGs were measured conventionally.[33,34] Small ERGs were anticipated in *Lca5*$^{gt/gt}$ mice, and thus the starting intensity for each of the series was set at ∼2 log units above the threshold response of wild-type mice.[18] Three mice developed corneal opacities after ERG testing and were excluded from subsequent pupillometry analyses. Transient pupillary light reflexes were recorded using a NeurOptics A-2000 (NeurOptics, Irvine, CA, USA) small animal pupillometry system as previously described.[18] The subset of mice receiving bilateral injections (AAV-hLCA5 or excipient) were used for TPLR analysis, to avoid confounding of the treated eye causing a contralateral pupil constriction in the untreated eye. The amplitude of pupillary constriction was measured in response to a series of five 40-ms 1000 and 3000 lux flashes per eye in anesthetized, dark-adapted mice and was defined as the difference between the baseline pupil diameter and the diameter obtained 0.6 to 1.2 seconds after stimulus onset.

Histology and Immunofluorescence. Eyes were enucleated, fixed in 4% paraformaldehyde, sectioned, and stained with hematoxylin and eosin using standard protocols. Slides were scanned using an Aperio AT2 Digital Pathology Slide Scanner at original magnification × 20 under brightfield illumination (Leica Microsystems) and analyzed using Aperio ImageScope software (Leica Microsystems). Images were exported as TIF files into image analysis software (http://imagej.nih.gov/ij/links.html) for retinal layer segmentation and quantification. ONL thickness was defined as the distance between the outer limiting membrane and the outer plexiform layer and was measured at locations that corresponded with the locations used for the OCT measurements. Measurements were averaged and plotted as mean values ±2 SD. For immunofluorescence studies, 12-µm frozen sections were incubated with anti- LCA5 (1:200; Proteintech, Rosemont, IL, USA), and anti-Rhodopsin antibodies (1:1000; Abcam, Cambridge, MA, USA), and ProLong Gold Antifade Mountant with DAPI (Thermo Fisher Scientific, Waltham, MA, USA). Slides were imaged with an Axio Imager M2 microscope (Zeiss, Oberkochen, Germany) equipped with epifluorescence and Axio-Vision 4.6 software.

Statistical Analysis. Statistical analysis was performed using GraphPad Prism 8.2.0 (GraphPad Software, Inc; La Jolla, CA, USA). Data distribution was assessed using the D'Agostino-Pears test. Differences in retinal layer thickness, ERG testing, and pupillary responses between AAV8-h*LCA5*-injected eyes and control eyes at P5, P15, and P30 were analyzed by one-way analysis of variance with a Bonferroni correction. A P value <.05 was considered significant (indicated in the figures by $^{*}P < 0.05$, $^{**}P < 0.01$, and $^{***}P < 0.001$).

Results

LCA5-LCA: One of the Most Severe Early-Onset Inherited Retinopathies

Five patients carrying homozygous null mutations in *LCA5* were included in the study (Table). Patients presented with reduced vision and nystagmus within the first year of life. Visual acuity was limited to light perception (LP) in three patients, 20/300 in one patient, and 20/500 in the remaining patient, in each eye. When measured, refractive errors were hyperopic (Table). To the best of our knowledge this level of vision has been present since diagnosis. All patients had prior ERG testing that was reported as nondetectable. En face imaging on patient 5 (P5), the oldest patient in the cohort, illustrates the abnormalities (Fig. 1A). There were pigmentary changes within the macula, but the pericentral and peripapillary retina had a better coloration (Fig. 1A). Buried optic nerve drusen were evidenced by their hyperautofluorescence on SW-FAF (Fig. 1A, *white arrow*). The better-preserved coloration of the RPE in these regions colocalizes with better preserved melanin-originating signals on NIR-FAF (Fig. 1A, *yellow arrows*). A range of pigmentary changes with better preservation of the pericentral and peripapillary retina were documented in the remainder of the patients (Fig. 1B). A yellow coloration of the fovea, more pronounced than expected for the normal macular pigment, was observed in at least one patient (Fig. 1B, *P3*).

Figure 1C illustrates and expands the reported spectrum of central SD-OCT structural abnormalities in *LCA5*-LCA, ranging from the least severe (P5, age 31) with a clearly detectable, albeit thin ONL band extending throughout the central scan, to the most severe (P3, age 21) with foveal atrophy and interruption of the RPE band (Fig. 1C, *asterisk*) with posterior displacement of the ocular layers.[6,11,12] The ONL could be detected at the fovea and in the peripapillary retina of the most affected patient. Individual OCT scans from at least one eye of each patient demonstrated

Investigative Ophthalmology & Visual Science

Table. Clinical and Molecular Characteristic of the Patients

Pt	Age/Gender	Age at Diagnosis	Ancestry	*LCA5* Mutations[†]	Mutation Type	Visual Acuity[‡]		Refraction[§]	
						OD	OS	OD	OS
P1	6/F	8 months[*]	Pakistani	Asn383del/Asn383del	Null/Null	LP	LP	np	np
P2	11/F	7 months[*]	Chinese	Gln421Stop/Gln421Stop	Null/Null	20/500	20/500	+6.25	+5.37
P3	21/F	2 years[*]	Indian	Asn383del/Asn383del	Null/Null	LP	LP	+2.75	+2.75
P4	22/M	3 months[*]	Lithuanian	Gln279Stop/Gln279Stop	Null/Null	LP	LP	np	np
P5	31/M	10 months[*]	Egyptian	Ser515Lys/Ser515Lysfs*78	Null/Null	20/300	20/300	+2.75	+3.50

[*] Nystagmus present within first 6 months of life.
[†] Predicted amino acid change; Allele 1/Allele 2.
[‡] Measured with Snellen charts; LP, light perception.
[§] Spherical equivalent; np = not performed.

detectable photoreceptors (ONL) in the central and midperipheral retina in all patients (Supplementary Fig. 1). We were unable to capture an image through the fovea in the youngest patient (P1; age 6) because of nystagmus and limited patient cooperation. A vertical scan in this patient clearly shows a thinned continuous ONL extending from the pericentral to the midperipheral retina (Supplementary Fig. 1). Signals superficial to the RPE that may correspond to abnormal but preserved photoreceptor inner segments, outer segments, or both, are visualized at the fovea with the help of LRPs in P5. The inner retina appears normal or thickened. To confirm detection of residual photoreceptors, LRPs were generated from the four patients (P2–P5) who had scans crossing the fovea (Fig. 1D). LRPs from a location 1.5 mm nasal to the foveal center, which showed possible presence of photoreceptors in all patients, were aligned vertically by the RPE signal peak and compared with a representative normal subject at that location (Fig. 1D). In the normal LRP the ONL can be identified as a trough between the signal peak of the OPL and RPE (Fig. 1D, *blue segment*). In all patients a clear trough in the reflectivity signal was present bracketed by signal peaks from the RPE and the OPL. P2 and P3 showed an additional small signal peak that may correspond to remnant signals from the inner (EZ band) or outer segments or both (Fig. 1D, *asterisks*). Of note, clear outer retinal sublaminae (EZ, IZ) present at the foveal center in P5 were not detectable in pericentral nasal retina.

Dark-adapted FST sensitivities to chromatic stimuli in patients who could reliably complete testing (P2, P4, P5) were reduced by at least 4.5 log units (range 4.5 to 5.5 log units; 467 nm) compared with normal values (Fig. 1E). Sensitivity differences between the red and blue stimulus were used to determine photoreceptor mediation.[21] Despite severely reduced sensitivities there was evidence of rod detection of the stimuli in the youngest patient in which measurements were possible (P2). The other two patients show evidence of cone-mediated detection. TPLR objectively confirmed the FST thresholds and provided a sensitivity estimate in a patient who could not reliably perform FST. TPLR thresholds were elevated on average by 5.1 log units (3.6 to 7.1 log units, with 467 nm light stimuli). Of the 2 patients who had both FST and TPLR (P2 and P4), thresholds were within 0.5 log units of each modality.

Natural History of Photoreceptor Degeneration in the *Lca5*$^{gt/gt}$ Mouse

The natural history of retinal degeneration of the *Lca5*$^{gt/gt}$ mouse,[16] was assessed by histologic retinal sections and SD-OCT imaging at P15, P30, and P60 (Figs. 2A–2C). *Lca5*$^{gt/gt}$ mice had a slightly decreased ONL thickness (85% of wild-type) (Fig. 2C; ONL highlighted in blue) on OCTs at P15 (mean ± 2SD = 59.9 ± 4.7 µm; n = 4) compared with age-matched wild-type mice (70.5 ± 5.4 µm; n = 8) (Figs. 2A–2D). The ellipsoid zone (EZ) and photoreceptor interdigitation zone (IZ) were no longer detectable in P15 *Lca5*$^{gt/gt}$ mice compared with wild-type mice (Fig. 2B, lines "2" and "3"). By P30, the ONL had thinned to about one third the thickness (22.5 ± 8.94 µm; n = 13) of wild-type mice (61.9 ± 4.9 µm; n = 6), and by P60 the ONL was undetectable (n = 10) (Figs. 2A–2D). There was no difference in inner retinal thickness in the *Lca5-d*eficient versus wild-type mice at P15, P30, or P60 (Figs. 2A–2D). The histologic measurements of ONL thickness corresponded closely with the OCT measurements in *Lca5*$^{gt/gt}$ mice; at P15 the ONL was 59.6 ± 11.7µm (n = 4), which became quickly thinned by P30 (17.9 ± 6.0 µm; n = 4) and reduced to a single layer of nuclei at P60 (3.2 ± 1.8; n = 4) (Figs. 2A, 2D). In contrast, the ONL thickness in wild-type mice remained 60.5 ± 8.3 µm (n = 6) at P60 (Figs. 2A, 2D).

ERG recordings were performed in age-matched wild-type and *Lca5*$^{gt/gt}$ mice as described above. Dark-adapted responses to an intensity series revealed detectable but decreased ERGs in 30-day old *Lca5*$^{gt/gt}$ mice compared with wild-type (Figs. 2E–2H). Rod-mediated responses elicited with a relatively dim flash (0.1 cd.s.m^{-2} stimulus) in 30-day-old *Lca5*$^{gt/gt}$ mice were ~10% (31 ± 23 µV) of the amplitudes of wild-type controls (365 ± 181 µV) (Figs. 2E, 2F). Dark-adapted ERGs elicited by a brighter stimulus (90 cd.s.m^{-2}) in *Lca5*$^{gt/gt}$ mice were slightly larger at ~20% (123 ± 62 µV) compared with wild-type animals (664 FµV ± 230 µV), suggesting a possible contribution of cone-mediated ERGs to this response (Figs. 2E, 2F). In anticipation of small ERG signals in *Lca5*$^{gt/gt}$ mice, additional ERG flicker protocols were used to allow greater averaging of the responses to improve the signal-to-noise ratio. Two frequencies were selected that are expected to be dominated by rods (4 Hz) or cones (10 Hz) in wild-type mice.[33] Dark-adapted 4-Hz flicker responses to the dim 0.1 cd s/m^2 stimulus in 30-day-old *Lca5*$^{gt/gt}$ mice were ~16% (49± 33 µV) of wild-type (262 ± 54.5 µV) mice (Figs. 2G, 2H). Dark-adapted 10-Hz flicker responses to the same stimulus (0.1 cd.s.m^{-2}) in *Lca5*$^{gt/gt}$ mice did not change in amplitude with increasing frequency as expected for wild-type animals, suggesting that dark-adapted ERGs may be dominated by cone-mediated responses in *Lca5*$^{gt/gt}$ animals (Figs. 2G, 2H). ERGs were reduced to ~15% (25 ± 15 µV) the amplitude of wild-type responses (161 ± 86 µV). By P60, ERGs were nondetectable in *Lca5*$^{gt/gt}$ mice in response to any of the stimulating

Investigative Ophthalmology & Visual Science

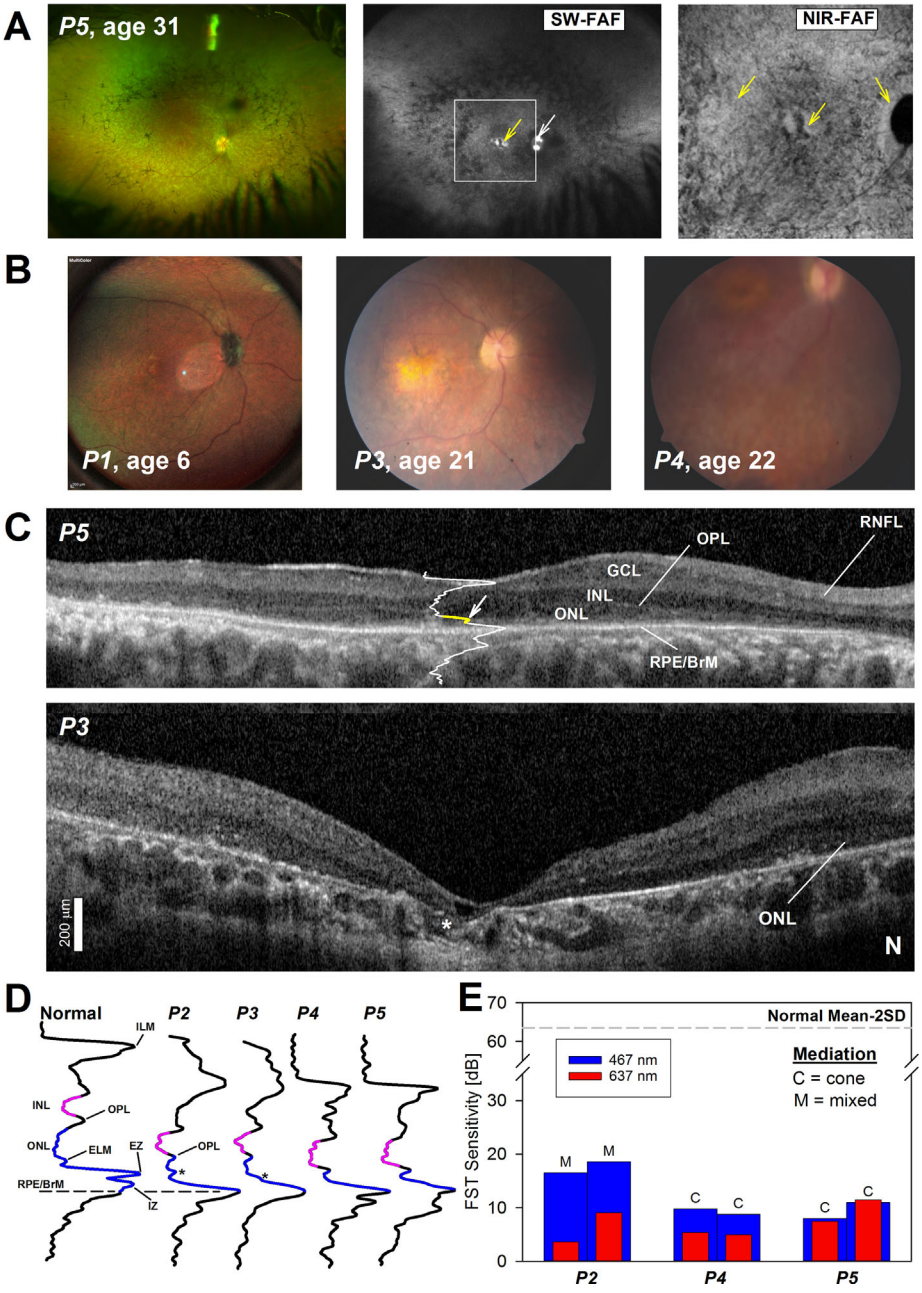

Figure 1. Retinal structure and function in patients with *LCA5*-associated LCA. **(A)** Wide-field fundus photography and SW-FAF and 30° near-infrared autofluorescence (NIR-FAF) imaging; *white square* in the SW-FAF image outlines the region imaged with NIR-FAF. *White arrow* indicates autofluorescent buried optic nerve drusen. *Yellow arrows* point to regions of better preserved SW- and NIR-FAF indicative of preserved lipofuscin and melanin-originating signals, respectively. **(B)** Multicolor scanning laser ophthalmoscope (SLO) (Heidelberg HRA) imaging (left panel) and conventional color fundus photos (central and right panel) reveals optic nerve pallor, vascular attenuation, and a midperipheral pigmentary retinopathy with variable preservation of the pericentral and peripapillary retina and a yellow discoloration of the fovea (*P3*). **(C)** Non-straightened, 9 mm-long SD-OCT cross-sections along the horizontal meridian through the fovea from nasal (N) retina in the least severe (*P5*, age 31) and most severe (*P3*, age 21) patients. Nuclear layers (ganglion cell layer, GCL; inner nuclear layer, INL; outer nuclear layer, ONL), outer plexiform layer (OPL) and a preserved retinal nerve fiber layer (RNFL) are labeled. Overlaid on *P5* is a longitudinal reflectivity profile (LRPs); yellow segment in the LRP indicates raise of signal from the external limiting membrane to the signal peak (*white arrow*) that corresponds to the ellipsoid zone (EZ) band. *Asterisk* in *P3* denotes interruption of RPE/BrM with posterior displacement of the retinal layers. **(D)** LRPs from 4 patients from a location 1.5 mm nasal to the foveal center, aligned vertically by the RPE/BrM signal peak and compared to a representative normal subject. Pink segment = INL; blue segment = outer retina (OPL to RPE/BrM); *asterisks* = remnant signals from the photoreceptor inner and/or outer segments (EZ band). The inner retina (ILM to OPL) is relatively thick in the patients. **(E)** Dark-adapted full-field stimulus testing (FST) sensitivities to chromatic stimuli (*blue bars* = 467 nm; *red bars* = 637 nm) in three patients who could complete testing. Pairs of bars plot sensitivities for the right (left bar) and left (right eye) for each patient. *Dashed line* = lower limit of normal for the 467 nm stimulus; spectral sensitivities were used to determine photoreceptor mediation (M = mixed rod and cone mediation; C = cone-mediated).

Investigative Ophthalmology & Visual Science

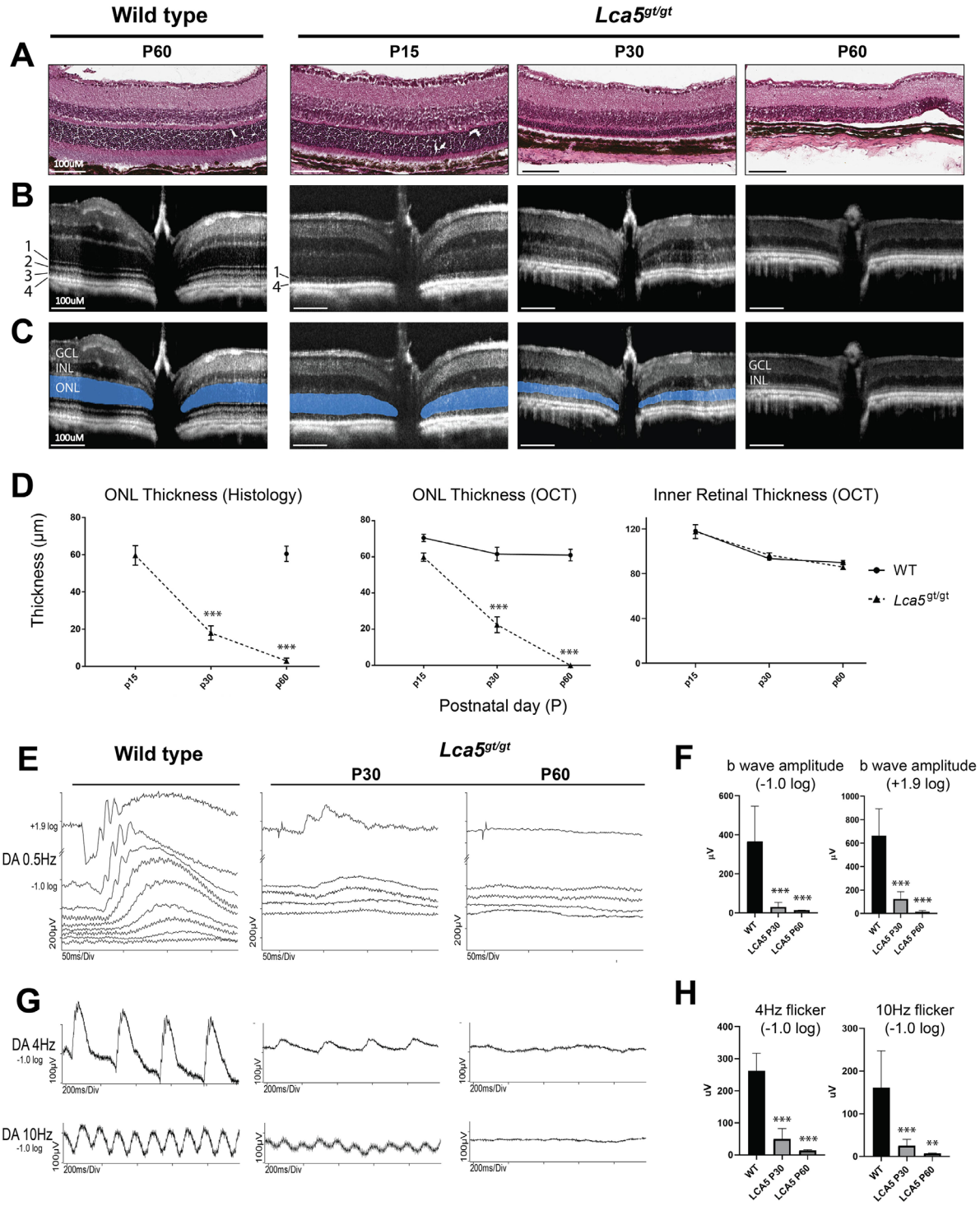

Figure 2. *Lca5*$^{gt/gt}$ mice have a rapid loss of photoreceptor structure and function. **(A)** Histologic retinal sections from wild-type (WT) vs. *Lca5*$^{gt/gt}$ mice at P15, P30, and P60 stained with hematoxylin and eosin (H&E) show a progressive loss of outer retinal structures: photoreceptor outer segments are shortened by P15, outer nuclear layer (ONL) is thinned by P30, and ONL is reduced to a single layer of nuclei by P60. **(B)** Horizontal SD-OCT sections through the optic nerve in WT and *Lca5*$^{gt/gt}$ mice. Outer retinal laminations: 1 = external limiting membrane (ELM), 2 = ellipsoid zone (EZ), 3 = interdigitation zone (IZ), 4 = RPE. By P15, only the ELM and RPE bands remain detectable. **(C)** Images in (B) with the ONL highlighted in blue highlight the loss of detectable ONL by P60. GCL = ganglion cell layer, INL = inner nuclear layer. Scale bars = 100 µm. **(D)** Quantification of ONL thickness by histology and SD-OCT from measurements 200 µm nasal and temporal to the optic nerve, compared to inner retinal thickness measured from OCTs at the same location. **(E)** Dark-adapted full-field electroretinogram (ERG) recordings performed in P60 wild-type and P30 and P60 *Lca5*$^{gt/gt}$ mice in response to an intensity series of stimuli reveals detectable signal in P30 but not in P60 *Lca5*$^{gt/gt}$ mice. **(F)** Quantification of ERG b wave amplitudes in response to a dim (-1.0 log scot-cd.m^2.s) and bright (+1.9 log scot-cd.m^2.s) stimulus. **(G)** Dark-adapted full-field ERG recordings in response to 4Hz (upper panel) and 10Hz (lower panel) flicker show an attenuated response in P30 *Lca5*$^{gt/gt}$ mice and isoelectric recordings in P60 animals. **(H)** Quantification of ERG flicker amplitudes in response to a 4Hz and 10Hz dim (-1.0 log scot-cd.m^2.s) stimulus. ***$P < 0.001$. *Error bars* are ± 2SD.

Investigative Ophthalmology & Visual Science

conditions, thus confirming a remarkably fast photoreceptor degeneration in this model (Figs. 2E–2H).

AAV8-*hLCA5* Gene Therapy Arrests Photoreceptor Loss in Early but not Late Stage Retinal Degeneration in the *Lca5*$^{gt/gt}$ mouse

To assess the window for therapeutic intervention for *LCA5*-LCA, we injected *Lca5*$^{gt/gt}$ mice subretinally at early- (P5, n = 12 eyes), mid- (P15, n = 14), and late-stage (P30, n = 15) photoreceptor degeneration with either an AAV8 vector containing the full-length wild-type native human *LCA5* cDNA or an injection of excipient-only (PBS with 0.001% Pluronic F68) control (P5, P15, P30, n = 30). OCT imaging could not be performed in eyes with lens opacities, including one eye injected at P5 and two eyes injected at P30 (Supplementary Table 1). The longevity of the treatment was assessed by examining these mice after treatment at P30 (for those treated before P30) and P60 (Figs. 3A, 3B). Failed resolution of the therapeutic retinal detachments led to persistent, localized, retinal detachments, which occurred more frequently when subretinal injections were performed in neonatal (P5) mice compared with older mice: 82% of P5-treated mice (9/11 eyes), 14% of P15-treated mice (2/14 eyes), and 8% of P30-treated mice (1/13 eyes). The retinal detachments visualized on OCT at P30 remained detached at P60 but did not interfere with subsequent imaging or testing.

Figure 3B shows representative horizontal OCT cross-sections through the optic nerve in *Lca5*$^{gt/gt}$ mice treated at P5, P15, or P30 and imaged after treatment at P30 and P60. Wild-type, uninjected *Lca5*$^{gt/gt}$ and excipient-injected eyes are shown at the same time-points for comparison (Figs. 3A, 3B). Inspection of the OCT scans at P30 demonstrates a variably thinned but clearly detectable ONL in all groups. There are no obvious differences in thickness of the ONL between the treated *Lca5*$^{gt/gt}$ animals and the uninjected *Lca5*$^{gt/gt}$ or excipient-injected controls. At P60, however, eyes treated with AAV8-*hLCA5* at P5 or P15 show an obvious ONL band, whereas animals injected at P30, excipient-injected, and uninjected *Lca5*$^{gt/gt}$ controls have no detectable ONL (Fig. 3B).

We quantified the results by determining the fraction of eyes that had a detectable ONL in peripapillary retina at each time point (P30 and P60). At P30, all groups had detectable ONL: 100% of uninjected *Lca5*$^{gt/gt}$, 88.9% of excipient-injected, 80% of P5-treated, and 100% of P15-treated animals (Fig. 3C). In contrast, at P60 none of the uninjected *Lca5*$^{gt/gt}$ (n = 8) or excipient-injected (n = 30) animals had any detectable ONL by OCT (Fig. 3D). In the treated groups at this time point (P60), 63.6% (7/11 eyes) of P5-treated animals and 57.1% 8/14 eyes) of P15-treated animals, but none (0/13 eyes) of the P30-treated animals had detectable ONL, suggesting that early treatment at P5 and P15 is more effective than treatment at P30 (Fig. 3D). Next, in the mice with detectable ONL, we measured the ONL thickness (200 µm from the optic nerve margin) in each eye of the different experimental groups at P30 and P60. Wild-type animals had an ONL thickness of 62.0 ± 4.9 µm (n = 6) at P30, which remained unchanged (60.5 ± 8.3 µm; n = 6) by P60 (Fig. 3E). The ONL in uninjected *Lca5*$^{gt/gt}$ mice at P30 was about a third the thickness of the wild-type animals (22.5 ± 4.5 µm; n = 13) at P30 and became undetectable (n = 6) by P60 (Fig. 3E). Remarkably, in the treated cohorts, P5-treated *Lca5*$^{gt/gt}$ mice maintained an ONL thickness equivalent to about one third of the wild-type thickness (18.9 ± 7.7 µm; n = 7) by P60, whereas P15-treated mice showed a slightly thinner ONL (12.4 ± 5.9 µm, n = 8) at P60. On the other hand, P30-treated *Lca5*$^{gt/gt}$ mice had undetectable ONL by OCT (n = 9) at P60, similar to untreated animals (Fig. 3E).

To ensure that the structural retinal preservation seen in the P5- and P15-treated *Lca5*$^{gt/gt}$ mice corresponded to regions of expression of the human LCA5 protein (Lebercilin), we performed immunofluorescence staining using antibodies specific to human LCA5. In control (excipient only) *Lca5*$^{gt/gt}$ animals, there was a single remaining row of ONL, no detectable LCA5 staining, and a thin band of rhodopsin expression just distal to the ONL (Fig. 4, *upper panel*), contrasting with the strong LCA5 immunostaining pattern reported in wild-type mice.[18] In P5- and P15-treated animals there were 3 to 6 layers of nuclei in the ONL, distinct regions of human LCA5 expression in both inner and outer retinal cells, and rhodopsin staining in photoreceptor outer segments of LCA5-positive and adjacent LCA5-negative photoreceptors (Fig. 4, *middle panels*; LCA5 expression in *green*, outer segments in *red*). P30-treated animals had a rudimentary layer of ONL similar to control animals, patchy expression of LCA5 in primarily outer retinal but not inner retinal cells, and distinct but scattered rhodopsin staining in a few cells distal to the ONL and in close proximity to the RPE (Fig. 4, *lower panel*).

ERGs were performed to determine whether the relatively preserved retinal structure documented in the P5- and P15-treated animals resulted in improved retinal function. When tested at P30, both P5- and P15-treated mice had measurable dark-adapted ERG responses to both single flash (+1.9 log scot-cd.s.m^{-2}) and flicker (4Hz and 10Hz; −1.0 log scot-cd.s.m^{-2}) stimuli (Fig. 5A). Untreated *Lca5*$^{gt/gt}$ mice, however, can have small detectable ERGs at P30 but are always nondetectable by P60 (Fig. 5A). When evaluated at P60, two of seven P5-treated mice with detectable ONL and one of eight P15-treated mice with detectable ONL had measurable, albeit reduced ERG signals. In contrast, P30-treated mice had no reliably detectable ERGs to any stimulus condition. Quantification of the average b-wave amplitude, however, did not show a statistically significant difference between the treated and untreated groups at P60, suggesting that the degree or extent of photoreceptor rescue in P5- and P15-treated animals was not sufficient in extent or magnitude to cause a significant change in retina-wide measures of function such as the full-field ERG (Fig. 5B). Locally efficacious treatment effects may thus be diluted by the combination of full-field ERG signals from responsive and unresponsive retina, whereas signal integration over large retinal areas by the pupillary light reflect allows detection of small changes in function of even small retinal regions.[35] With this in mind we measured the TPLR in treated and untreated *Lca5*$^{gt/gt}$ mice in response to 1000 and 3000 lux stimuli and found that P5- and P15-treated mice had larger TPLR responses compared with P30-treated, untreated, and excipient-only (excipient pooled from all injection time points) mice (Fig. 5C and 5D). TPLR constriction amplitudes expressed as a fraction of the baseline pupil diameter for each of the two light stimuli showed a graded TPLR response, with the greatest response in P5-treated animals (15%-17%), a moderately preserved response in P15-treated animals (~12%), and minimally detectable pupillary responses in P30-treated (<3%) and uninjected *Lca5*$^{gt/gt}$ control animals (<5%) (Figs. 5C, 5D).

Investigative Ophthalmology & Visual Science

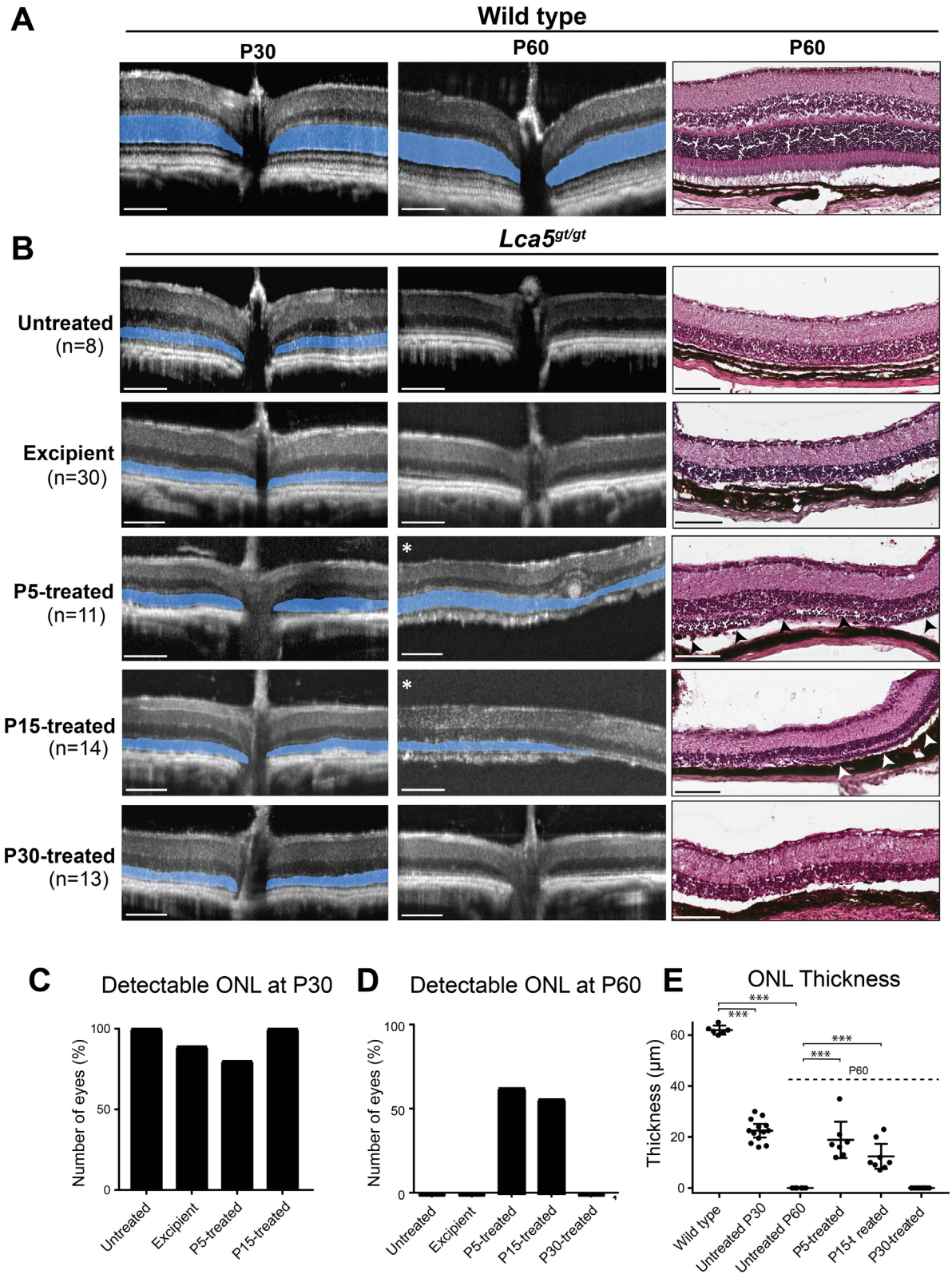

Figure 3. Gene therapy preserves ONL structure when delivered to P5 and P15, but not P30 *Lca5*$^{gt/gt}$ mice. **(A)** Horizontal SD-OCT sections through the optic nerve in P30 and P60 wild-type (WT) mice; ONL highlighted in blue. Corresponding histologic section stained with hematoxylin and eosin (H&E). **(B)** Horizontal SD-OCT sections through the optic nerve in untreated, excipient-treated controls, P5-treated, P15-treated, and P30-treated *Lca5*$^{gt/gt}$ mice imaged at P30 (*left column*) and P60 (*center column*). ONL is highlighted in blue and is no longer detectable in untreated or excipient-treated controls by P60. P5-treated and P15-treated animals have regions of preserved ONL by P60 (*asterisks*) that corresponds to detectable ONL on histologic sections (*right column, arrowheads*) within the site of subretinal injections. Scale bars = 100 µm. **(C, D)** Percent of eyes with detectable ONL at P30 **(C)** and P60 **(D)**; only the P5-treated and P15-treated mice have remaining ONL at P60. **(E)** Quantification of ONL thickness in WT and untreated animals (200 µm nasal and temporal to the optic nerve), and within the subset of treated animals with detectable regions of ONL at the site of the subretinal injection in treated animals at a location that corresponds to the nasal measurements. ***$P < 0.001$. Error bars are ± 2SD. Dashed line = groups measured at P60.

Investigative Ophthalmology & Visual Science

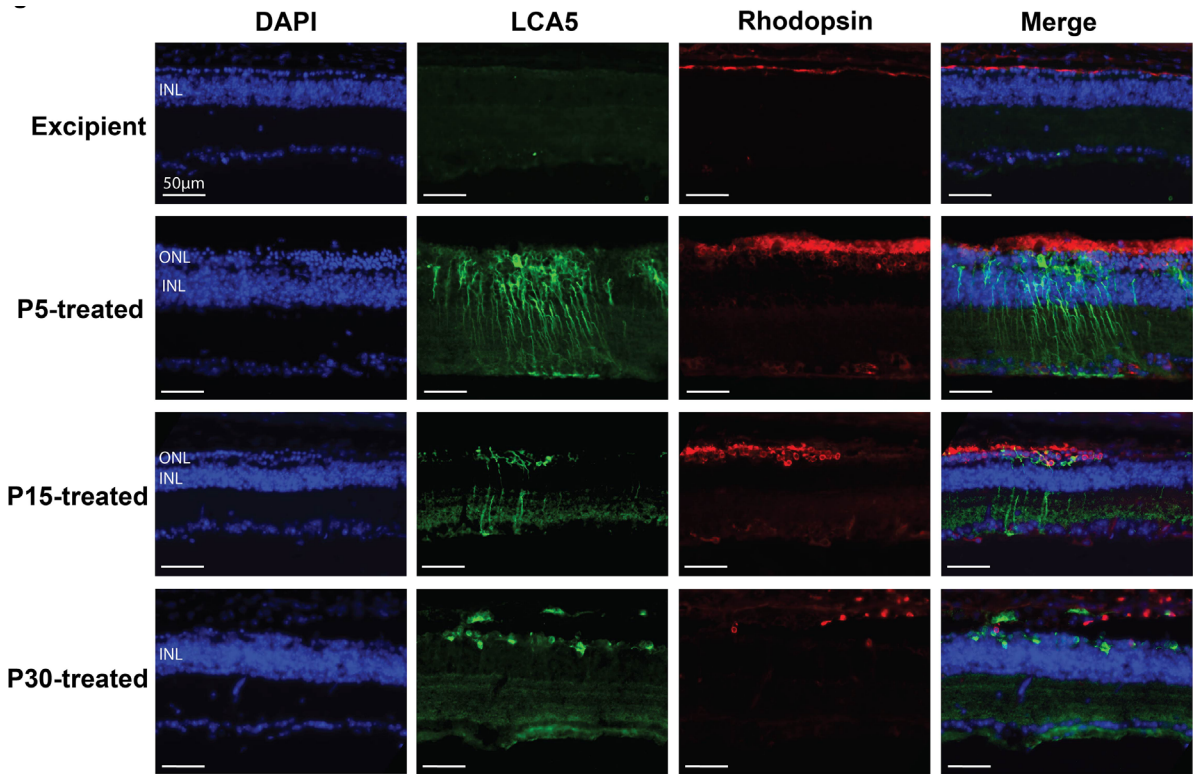

Figure 4. Immunofluorescence staining of LCA5 (*green*), rhodopsin (*red*, labels photoreceptor outer segments), and nuclei (*blue*) of excipient-injected control animals, P5-treated, P15-treated, and P30-treated *Lca5*$^{gt/gt}$ mice harvested at P90; merged images shown to the right. LCA5 expression within sites of the subretinal AAV injection corresponds with regions of ONL preservation and rhodopsin expression, suggestive of structurally intact photoreceptors at these locations. No ONL or rhodopsin expression is seen in P30-treated animals. INL = inner nuclear layer; ONL = outer nuclear layer. Scale bars = 50µm.

We next sought to extrapolate results of these murine data to determine whether there is a window of opportunity for treatment in human *LCA5*-LCA patients. ONL thickness measured in vivo with SD-OCT in treated *Lca5*$^{gt/gt}$ mice and expressed as a fraction of the location-specific mean normal thickness demonstrates that unequivocal treatment success in P15-injected (or earlier) corresponds to retinas with a peripapillary ONL thickness that is at least ~85% of normal thickness at the time of injection (and presumably less at the time of AAV gene expression ~5 days later) (Fig. 6, *green symbols*). P30-treated animals with questionable or no signs of rescue at P60 by TPLR (Fig. 5C) showed ONL thicknesses that were reduced to at least 30% of normal (Fig. 6, *black symbols*). If photoreceptor loss as measured is the main determinant of treatment potential, and assuming the fast photoreceptor degeneration in *Lca5*$^{gt/gt}$ mice follows a linear decay between the two time points of treatment (P15 and P30), then a therapeutic window may still exist for animals with severe photoreceptor degeneration as long as their residual ONL thickness is greater than 30% of normal (Fig. 6). It follows that treatment efficacy may be achievable in some *LCA5*-LCA patients in regions where degeneration still spares photoreceptors to at least 30% of their normal complement. Residual islands of photoreceptors in the pericentral retina of *LCA5*-LCA patients in this study were about half the normal thickness (Fig. 6, *red symbols*), equivalent to levels of photoreceptor degeneration in the *Lca5*$^{gt/gt}$ mouse before P30.

Discussion

In the spectrum of severe early-onset retinal degenerative conditions, *LCA5*-LCA ranks as a particularly severe disease with profound vision loss and central structural abnormalities detected from early childhood.[1–10,12–15,36] Consistent with previous reports we found a severe photoreceptor degeneration with areas of relatively preserved outer pericentral retina and variable foveal abnormalities in all patients.[2,11,37] There was no clear relationship between the specific genotype or age and the severity of phenotype in our patients, analogous to several other forms of LCA.[38–40] Although our youngest patient (6 years old) showed the largest expanse (into the midperiphery) of detectable photoreceptors in *LCA5*-LCA reported to date, our oldest patient (age 31) also showed remarkable central photoreceptor preservation, equivalent to what has been reported with OCT for this disease.[6,12] Ages sampled between these two extremes in this work showed more severe examples of degeneration. Detecting a structural-functional dissociation, a reliable indicator of treatment potential in inherited retinal degenerations is challenging in *LCA5*-LCA. Unlike *RPE65*-LCA, for example, in *LCA5*-LCA there may be both severe retinal dysfunction and structural loss even in the youngest patients, which challenges treatment potential.[6,40–42] The relatively preserved retinas of some patients in this study (for example, P1 and P5) showed ONL thicknesses that were between 50% to 75% of the normal thickness values

Investigative Ophthalmology & Visual Science

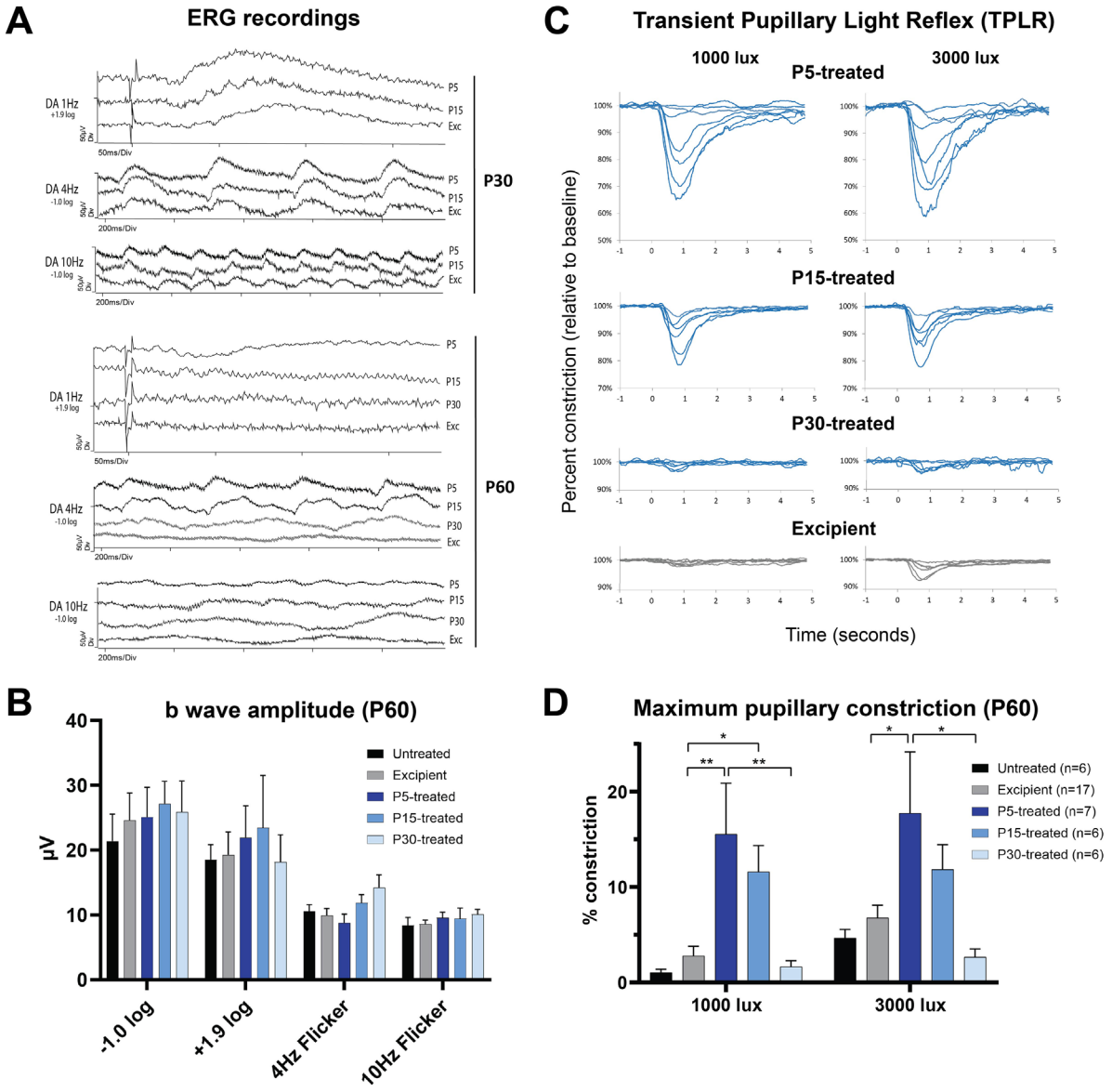

Figure 5. Functional rescue in P5- and P15-treated, but not P30-treated animals. **(A)** Dark-adapted full-field ERG recordings performed in P60 excipient-treated controls, P5-treated, P15-treated, and P30-treated *Lca5*$^{gt/gt}$ mice in response to 0.5Hz, 4Hz, and 10Hz stimuli at P30 (upper panel) and P60 (lower panel). At P30, ERG responses are detectable in all groups. By P60, tracings are isoelectric in all excipient-treated controls but show detectable responses in representative animals treated at P5 and P15, but not P30. **(B)** Quantification of full-field ERG b wave amplitudes in response to a 0.5Hz, 4Hz, and 10Hz dim (-1.0 log scot-cd.s.m^{-2}) stimulus and 1Hz bright (+1.9 log scot-cd.s.m^{-2}) stimulus. There is no statistically significant difference between the average amplitudes of untreated, excipient-treated, P5-, P15-, and P30-treated animals. Error bars indicate SEM. **(C)** Transient pupillary light reflex (TPLR) recordings were performed at P60 in control, P5-treated, P15-treated, and P30-treated *Lca5*$^{gt/gt}$ mice using stimulation with 1K and 3K scot lux m^2 (for 40 ms). Traces represent recordings from individual eyes, normalized to baseline pupil diameter. **(D)** Quantification of the maximum pupillary constriction (as a percent from baseline) in each cohort; excipient-injections were performed at P5, P15, and P30 as controls for each injection timepoint and all excipient responses were pooled for simplicity. *$P < 0.05$; **$P < 0.01$. *Error bars* are ± SEM.

for the most preserved locations, whereas FST sensitivity losses exceeded 4.5 log units. This supports a pattern of structural-functional dissociation previously hinted by pupillometric thresholds in this disease and raises hopes that gene augmentation may be able to restore some level of vision in these patients.[6]

The presence of regions of preserved RPE and photoreceptors well into adulthood also provides hope that this disease may be amenable to treatment in some patients into adulthood. Both rod- and cone-mediated sensitivities were documented by FST early in the disease in one of our youngest patients in this study, as well as residual cone vision late in the disease, a pattern of degeneration involving both rods and cone photoreceptors reminiscent of that observed in the *Lca5*$^{gt/gt}$ mouse model.[18] Measurable cone function in late-stage disease suggests relative resilience of cone photoreceptors to degeneration and the potential for their rescue by gene therapy. On the other hand, quantifiable visual function by FST and TPLR despite the severity of the disease supports the use of

Investigative Ophthalmology & Visual Science

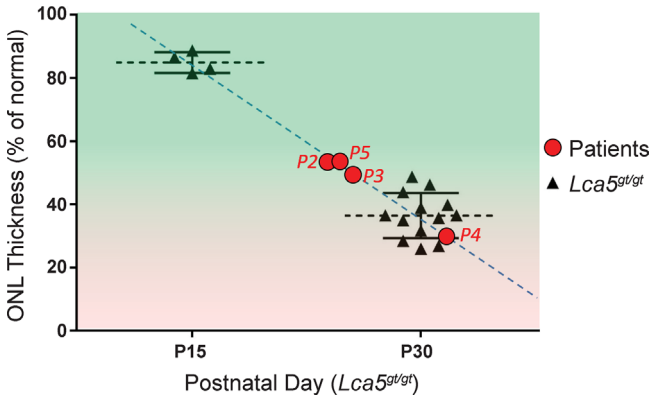

Figure 6. ONL thickness expressed as a percentage of the measures in wild-type mice at the same location for *Lca5*$^{gt/gt}$ mice treated at P15 and P30. ONL thickness declines dramatically in the *Lca5*$^{gt/gt}$ mouse, from 85% of wild-type at P15, to 37% of wild-type by P30; *diagonal green dashed line* models linear ONL loss between the two time points. *Horizontal dashed lines* represent the ONL mean thickness for each P15 and P30 group, solid lines represent ± SD. The colored background represents a theoretical gradient of functional improvement after gene therapy relating to the percentage of remaining ONL at the time of treatment, with green indicating preserved ONL and improved functional outcome, and red indicating loss of ONL and limited therapeutic potential. ONL thickness from best preserved regions in the pericentral retina of four *LCA5*-LCA patients expressed as a percentage of the location-specific normal mean value (*red symbols*). *P2*, *P3*, and *P5* had similar ONL thickness (54%, 52%, 54%, respectively) whereas P4 had a slightly thinner ONL (28%) similar to that of a P30 *Lca5*$^{gt/gt}$ mouse.

these measurements as outcome measures of the safety and efficacy of future interventions for this particularly severe disease, as has been the case for other forms of LCA, such as *RPE65*-LCA.[6,21,35,41–44] Future studies in this particular group of patients are needed to determine their performance in terms of reliability and reproducibility before the tests are fully endorsed as outcome measures for future clinical trials. It is possible that objective measures of structural change may take a dominant role in this scenario, a picture quite different from that expected at the initiation of the *RPE65*-LCA gene therapy trials.

We sought to characterize the natural history of photoreceptor degeneration in the mouse model of *LCA5*-LCA to draw parallels with the human disease with the ultimate goal of assessing the potential efficacy and time windows of treatments in patients. We report the first quantitative temporal analysis of retinal degeneration in the *Lca5*$^{gt/gt}$ mouse model using noninvasive retinal imaging (OCT), a technique widely used in ophthalmology clinics. We show that OCT provides an accurate measurement of ONL thickness and that the *Lca5*$^{gt/gt}$ mouse model replicates the fast and early photoreceptor degeneration observed in patients. ONL quantification by OCT revealed a fast-progressing retinal degeneration with outer segment loss at the earliest time-point (Fig. 2B, P15), detectable ONL thinning between P15 and P30, and total loss of photoreceptors within the sampled regions by P60. These measurements were verified by quantification of ONL thickness on histologic sections. The ONL thickness of *Lca5*$^{gt/gt}$ mice was decreased by 15% compared with wild-type animals at P15 and decreased by almost 70% of wild-type thickness at P30. Interestingly, residual rod- and cone-mediated ERG signals were barely detectable at this stage despite the fact that one third of the photoreceptors were clearly detectable, suggesting a disproportionate loss of retinal function compared with measurable structure, an expected phenotype in some forms of LCA.[40,42,45] Admittedly, sampling the peripapillary retina by OCT in this model assumes homogenous loss across the entire retina and may, in fact, overestimate or underestimate the level of photoreceptor preservation contributing to the full-field ERG. The pattern of loss involving rod and cone photoreceptors, as well as the possible dissociation between photoreceptor structure and function in the *Lca5*$^{gt/gt}$ mice, is also analogous with what we describe in the patients included in this study.

There is evidence that subretinal delivery of an AAV7m8 viral vector containing human *LCA5* cDNA can rescue the retinal structure and function when administered to *Lca5*$^{gt/gt}$ mice at P4 to P6.[18] Because of innate differences in the size, anatomy, and physiology of the rodent eye compared to the human eye, however, not all viral vectors that are effective in preclinical mouse studies can be directly translated to nonhuman primates (NHP) or to human clinical trials. Testing of AAV7m8 in the NHP eye, which has a cone-rich macula and most closely resembles the human eye, revealed decreased cellular expression and increased toxicity when compared to the safety and expression profile of this vector in the mouse.[30] Therefore we delivered wild-type *LCA5* using a well-characterized AAV8 serotype that has a more favorable safety and expression profile in both the mouse and NHP and thus may be more suitable for translation into human clinical studies.[28,29,46] Precipitous degeneration in a period of 1 month between P30 and P60 in the *Lca5*$^{gt/gt}$ mouse allowed us to unequivocally confirm partial rescue of the phenotype at P60 for treatments delivered before P30. At the fast rate of photoreceptor degeneration described for this model, it is still conceivable that lack of rescue for animals injected at ages >P30 may be a consequence of the added delay in initiation of protein expression after the delivery of gene therapy (approximately 5 days for AAV8), placing the potential beneficial effect beyond P30.[47] The longitudinal assessment of the TPLR and of the structural preservation with SD-OCT in *Lca5*$^{gt/gt}$ mice treated before P30 will help define both the longevity of treatment and its dependency on the level of photoreceptor degeneration, questions of critical importance for future clinical trials.[18,48]

Photoreceptor loss at P30 in the *Lca5*$^{gt/gt}$ mice is comparable to the level of photoreceptor loss observed in pockets of residual photoreceptors in the patients with the most severe disease described herein (P2, P3, P4), whereas locally milder disease in other patients (P1 and P5) suggests a level of preservation similar to that of the younger mice (P15) in which gene therapy-mediated rescue was possible. The findings suggest that treatment efficacy in patients will be related to the level of photoreceptor loss rather the age of the patients, although earlier intervention may be desirable to achieve efficacy as well as to prevent interference of the disease with retinal and retinocortical development, oculomotor stability, and emmetropization. The presence of detectable signals by SD-OCT that may correspond to preserved inner segments and proximal outer segments in this and a previous study raises hope that correction of the molecular defect in this ciliopathy may lead to restoration of the outer segment physiology and to improvements in function as has been recently documented for *CEP290*-LCA, a similarly severe ciliopathy.[49] Evaluations of larger groups of patients with *LCA5*-LCA both in cross-section and longitudinally are needed to confirm if these observations are generalizable. Overall, these findings suggest that *LCA5*-LCA

Investigative Ophthalmology & Visual Science

patients may benefit from gene augmentation therapies despite early-onset and uniquely severe retinal degeneration.

Acknowledgments

The authors thank the patients and their families for participation in this study. We thank Arkady Lyubarsky for assistance with mouse electroretinography and Junwei Sun for helpful discussions regarding the LCA5 vectors. We are grateful to Jieyan Pan and the CAROT Research Vector Core for production of the rAAV vector.

Supported by grants from Hope for Vision, The Foundation Fighting Blindness, Macula Vision Research Foundation, The Paul and Evanina Bell Mackall Foundation Trust, the Brenda and Matthew Shapiro Stewardship, the Robert and Susan Heidenberg Investigative Research Fund for Ocular Gene Therapy, The Pennsylvania Lions Sight Conservation and Research Foundation, and Research to Prevent Blindness. KU was supported by a NIH/NEI Institutional K12 Vision Clinical Scientist Program Grant 5K12EY015398-14.

Disclosure: **J. Bennett,** Spark Therapeutics (E), GenSight Biologics (I), Limelight Bio (I), Akouos (S), Odylia Therapeutics (S), Limelight Bio (F, P); **K.E. Uyhazi,** None; **P. Aravand,** None; **B.A. Bell,** None; **Z. Wei,** None; **L. Leo,** None; **L.W. Serrano,** None; **D.J. Pearson,** None; **I. Shpylchak,** None; **J. Pham,** None; **V. Vasireddy,** None; **T.S. Aleman,** None

References

1. Dharmaraj S, Li Y, Robitaille J, et al. A novel locus for Leber congenital amaurosis maps to chromosome 6q. *Am J Hum Genet*. 2000;66:319–326.
2. Mohamed M, Topping N, Jafri H, Raashed Y, McKibbin M, Inglehearn C. Progression of phenotype in Leber's congenital amaurosis with a mutation at the LCA5 locus. *Br J Ophthalmol*. 2003;87:473–475.
3. den Hollander AI, Koenekoop RK, Mohamed MD, et al. Mutations in LCA5, encoding the ciliary protein lebercilin, cause Leber congenital amaurosis. *Nat Genet*. 2007;39:889–895.
4. Gerber S, Hanein S, Perrault I, et al. Mutations in LCA5 are an uncommon cause of Leber congenital amaurosis (LCA) type II. *Hum Mutat*. 2007;28:1245.
5. Ramprasad VL, Soumittra N, Nancarrow D, et al. Identification of a novel splice-site mutation in the Lebercilin (LCA5) gene causing Leber congenital amaurosis. *Molecular Vision*. 2008;14:481–486.
6. Jacobson SG, Aleman TS, Cideciyan AV, et al. Leber congenital amaurosis caused by Lebercilin (LCA5) mutation: Retained photoreceptors adjacent to retinal disorganization. *Mol Vis*. 2009;15:1098–1106.
7. Coene KL, Roepman R, Doherty D, et al. OFD1 is mutated in X-linked Joubert syndrome and interacts with LCA5-encoded lebercilin. *Am J Hum Genet*. 2009;85:465–481.
8. Seong MW, Kim SY, Yu YS, Hwang JM, Kim JY, Park SS. LCA5, a rare genetic cause of leber congenital amaurosis in Koreans. *Ophthalmic Genet*. 2009;30:54–55.
9. McKibbin M, Ali M, Mohamed MD, et al. Genotype-phenotype correlation for Leber congenital amaurosis in Northern Pakistan. *Arch Ophthalmol*. 2010;128:107–113.
10. Ahmad A, Daud S, Kakar N, et al. Identification of a novel LCA5 mutation in a Pakistani family with Leber congenital amaurosis and cataracts. *Mol Vis*. 2011;17:1940–1945.
11. Mackay DS, Borman AD, Sui R, et al. Screening of a large cohort of Leber congenital amaurosis and retinitis pigmentosa patients identifies novel *LCA5* mutations and new genotype-phenotype correlations. *Human Mutation*. 2013;34:1537–1546.
12. Corton M, Avila-Fernandez A, Vallespin E, et al. Involvement of LCA5 in Leber congenital amaurosis and retinitis pigmentosa in the Spanish population. *Ophthalmology*. 2014;121:399–407.
13. Li L, Xiao X, Li S, et al. Detection of variants in 15 genes in 87 unrelated Chinese patients with Leber congenital amaurosis. *PLoS ONE*. 2011;6:e19458.
14. Abu-Safieh L, Alrashed M, Anazi S, et al. Autozygome-guided exome sequencing in retinal dystrophy patients reveals pathogenetic mutations and novel candidate disease genes. *Genome Res*. 2013;23:236–247.
15. Chen X, Sheng X, Sun X, et al. Next-generation sequencing extends the phenotypic spectrum for LCA5 mutations: Novel LCA5 mutations in cone dystrophy. *Sci Rep*. 2016;6:24357.
16. Boldt K, Mans DA, Won J, et al. Disruption of intraflagellar protein transport in photoreceptor cilia causes Leber congenital amaurosis in humans and mice. *J Clin Invest*. 2011;121:2169–2180.
17. den Hollander AI, Roepman R, Koenekoop RK, Cremers FP. Leber congenital amaurosis: Genes, proteins and disease mechanisms. *Prog Retin Eye Res*. 2008;27:391–419.
18. Song JY, Aravand P, Nikonov S, et al. Amelioration of neurosensory structure and function in animal and cellular models of a congenital blindness. *Mol Ther*. 2018;26:1581–1593.
19. Russell S, Bennett J, Wellman JA, et al. Efficacy and safety of voretigene neparvovec (AAV2-hRPE65v2) in patients with RPE65-mediated inherited retinal dystrophy: A randomised, controlled, open-label, phase 3 trial. *Lancet*. 2017;390:849–860.
20. Maguire AM, Russell S, Wellman JA, et al. Efficacy, safety, and durability of Voretigene Neparvovec-rzyl in RPE65 mutation-associated inherited retinal dystrophy: Results of phase 1 and 3 trials. *Ophthalmology*. 2019;126:1273–1285.
21. Aleman TS, Uyhazi KE, Serrano LW, et al. RDH12 mutations cause a severe retinal degeneration with relatively spared rod function. *Invest Ophthalmol Vis Sci*. 2018;59:5225–5236.
22. Aleman T, Morgan J, Serrano L, et al. Natural history of the central structural abnormalities in choroideremia: A prospective cross-sectional study. *Ophthalmology*. 2017;124:359–373.
23. Bonafede L, Ficicioglu CH, Serrano L, et al. Cobalamin C deficiency shows a rapidly progressing maculopathy with severe photoreceptor and ganglion cell loss. *Investigative Opthalmol Vis Sci*. 2015;56:7875–7887.
24. Roman AJ, Cideciyan AV, Aleman TS, Jacobson SG. Full-field stimulus testing (FST) to quantify visual perception in severely blind candidates for treatment trials. *Physiol Meas*. 2007;28:N51–N56.
25. Klein M, Birch DG. Psychophysical assessment of low visual function in patients with retinal degenerative diseases (RDDs) with the Diagnosys full-field stimulus threshold (D-FST). *Doc Ophthalmol*. 2009;119:217–224.
26. Bell BA, Kaul C, Hollyfield JG. A protective eye shield for prevention of media opacities during small animal ocular imaging. *Exp Eye Res*. 2014;127:280–287.
27. Bell BA, Bonilha VL, Hagstrom SA, Anand-Apte B, Hollyfield JG, Samuels IS. Prolonged ocular exposure leads to retinal lesions in mice. *Exp Eye Res*. 2019;185:107672.
28. Vandenberghe L, Bell P, Maguire A, et al. Dosage thresholds for AAV2 and AAV8 photoreceptor gene therapy in monkey. *Sci Transl Med*. 2011;3:88ra54.
29. Black A, Vasireddy V, Chung DC, et al. Adeno-associated virus 8-mediated gene therapy for choroideremia:

Preclinical studies in in vitro and in vivo models. *J Gene Med*. 2014;16:122–130.

30. Ramachandran PS, Lee V, Wei Z, et al. Evaluation of dose and safety of AAV7m8 and AAV8BP2 in the non-human primate retina. *Hum Gene Ther*. 2017;28:154–167.
31. Su Q, Sena-Esteves M, Gao G. Production of recombinant adeno-associated viruses (rAAVs) by transient transfection. *Cold Spring Harb Protoc*. 2020;2020:pdb prot095596.
32. Liang FQ, Anand V, Maguire AM, Bennett J. Intraocular delivery of recombinant virus. *Methods Mol Med*. 2001;47:125–139.
33. Seeliger MW, Grimm C, Stahlberg F, et al. New views on RPE65 deficiency: The rod system is the source of vision in a mouse model of Leber congenital amaurosis. *Nat Genet*. 2001;29:70–74.
34. Aleman T, LaVail M, Montemayor R, et al. Augmented rod bipolar cell function in partial receptor loss: An ERG study in P23H rhodopsin transgenic and normal rats. *Vision Res*. 2001;41:2779–2797.
35. Aleman TS, Jacobson SG, Chico JD, et al. Impairment of the transient pupillary light reflex in Rpe65(−/−) mice and humans with Leber congenital amaurosis. *Invest Ophthalmol Vis Sci*. 2004;45:1259–1271.
36. Mackay DS, Borman AD, Sui R, et al. Screening of a large cohort of leber congenital amaurosis and retinitis pigmentosa patients identifies novel LCA5 mutations and new genotype-phenotype correlations. *Hum Mutat*. 2013;34:1537–1546.
37. Maranhao B, Biswas P, Gottsch ADH, et al. Investigating the molecular basis of retinal degeneration in a familial cohort of Pakistani decent by exome sequencing. *Plos One*. 2015;10:e0136561.
38. Jacobson SG, Cideciyan AV, Sumaroka A, et al. Outcome measures for clinical trials of Leber congenital amaurosis caused by the intronic mutation in the *CEP290* gene. *Invest Opthalmol Vis Sci*. 2017;58:2609.
39. Jacobson SG, Aleman TS, Cideciyan AV, et al. Defining the residual vision in Leber congenital amaurosis caused by RPE65 mutations. *Invest Ophthalmol Vis Sci*. 2009;50:2368–2375.
40. Jacobson SG, Cideciyan AV, Sumaroka A, et al. Defining outcomes for clinical trials of Leber congenital amaurosis caused by GUCY2D mutations. *Am J Ophthalmol*. 2017;177:44–57.
41. Cideciyan AV, Rachel RA, Aleman TS, et al. Cone photoreceptors are the main targets for gene therapy of NPHP5 (IQCB1) or NPHP6 (CEP290) blindness: Generation of an all-cone Nphp6 hypomorph mouse that mimics the human retinal ciliopathy. *Hum Mol Genet*. 2011;20:1411–1423.
42. Cideciyan AV, Aleman TS, Jacobson SG, et al. Centrosomal-ciliary gene CEP290/NPHP6 mutations result in blindness with unexpected sparing of photoreceptors and visual brain: Implications for therapy of Leber congenital amaurosis. *Hum Mutat*. 2007;28:1074–1083.
43. Cideciyan AV, Aleman TS, Boye SL, et al. Human gene therapy for RPE65 isomerase deficiency activates the retinoid cycle of vision but with slow rod kinetics. *Proc Natl Acad Sci USA*. 2008;105:15112–15117.
44. Jacobson SG, Cideciyan AV, Aleman TS, et al. RDH12 and RPE65, visual cycle genes causing leber congenital amaurosis, differ in disease expression. *Invest Ophthalmol Vis Sci*. 2007;48:332–338.
45. Cideciyan AV. Leber congenital amaurosis due to RPE65 mutations and its treatment with gene therapy. *Progress in Retinal and Eye Research*. 2010;29:398–427.
46. Vandenberghe LH, Bell P, Maguire AM, et al. Dosage thresholds for AAV2 and AAV8 photoreceptor gene therapy in monkey. *Sci Transl Med*. 2011;3:88ra54.
47. Allocca M, Mussolino C, Garcia-Hoyos M, et al. Novel adeno-associated virus serotypes efficiently transduce murine photoreceptors. *J Virol*. 2007;81:11372–11380.
48. Gardiner KL, Cideciyan AV, Swider M, et al. Long-term structural outcomes of late-stage RPE65 gene therapy. *Mol Ther*. 2020;28:266–278.
49. Cideciyan AV, Jacobson SG, Drack AV, et al. Effect of an intravitreal antisense oligonucleotide on vision in Leber congenital amaurosis due to a photoreceptor cilium defect. *Nat Med*. 2019;25:225–228.

Investigative Ophthalmology & Visual Science